Earth Systems and Environment (2022) 6:221–235
https://doi.org/10.1007/s41748-021-00291-w

ORIGINAL ARTICLE

Investigating the Impact of Land Use/Land Cover Change on Present and Future Land Surface Temperature (LST) of Chittagong, Bangladesh

Shahriar Abdullah[1] · **Dhrubo Barua**[1] · **Sk. Md. Abubakar Abdullah**[2] · **Yasin Wahid Rabby**[3]

Received: 23 August 2021 / Revised: 23 December 2021 / Accepted: 28 December 2021 / Published online: 19 January 2022

Abstract
Urbanization has a significant impact on microclimate, which eventually contributes to local and regional climate change. Unplanned urbanization is widespread in developing countries like Bangladesh. Chittagong, the second largest city, is experiencing rapid urban expansion. Since urban growth introduces a number of environmental issues, including changes in land surface temperature (LST), it is important to investigate the association between urbanization pattern and LST in Chittagong. In this work, we have analyzed the influence of land use and land cover (LULC) of Chittagong Metropolitan Area (CMA) on LST using multi-date Landsat data of 1990, 2005 and 2020. We have used an artificial neural network (ANN) algorithm for LULC classification and an image-based method to compute LST from Landsat data. The results revealed that built-up areas, waterbodies and agricultural lands have increased by 4.57%, 1.04% and 0.94%, respectively, whereas vegetation has decreased by 0.34% and bare lands by 0.87% between 1990 and 2020. As expected, built-up area experienced maximum temperatures followed by bare lands. Waterbodies, on the other hand, exhibited minimum temperature in all years considered, followed by vegetation. Correlations between biophysical variables, Normalized Difference Vegetation Index (NDVI), Normalized Difference Built-up Index (NDBI), Modified Normalized Difference Water Index (MNDWI) and Bare Soil Index (BSI), and LST indicated that NDVI and MNDWI were in a strong negative relationship, whereas NDBI and BSI have showed positive correlation with LST. Lastly, LST is predicted based on the relationship between LST and biophysical variables with an ANN algorithm, which demonstrated that the temperature may reach to a critical state by 2050, if the present trend of urban growth continues.

Keywords Chittagong · LST · LULC · Biophysical variables · ANN

1 Introduction

Land cover alteration, driven by increased anthropogenic activities, is a common phenomenon across the world but the intensity is high in developing countries like Bangladesh (Wurm and Taubenböck 2018; Panday 2020). Many studies have investigated drivers behind rapid land use and land cover (LULC) change, and have showed that population growth (Dewan and Corner 2014a; El-Zeiny and Effat 2017; Yohannes et al. 2021), economic affluence (Karakuş 2019), industrialization and rural to urban migration (Mberu et al. 2017) are major reasons behind LULC modification. This modification evidently impacts the environment in various ways, including deforestation (Behera et al. 2018), pollution (Hua 2017), flooding (Rahman et al. 2021), biodiversity loss (Sharma et al. 2018) and local warming (Ullah et al. 2019). Temperature is directly influenced by LULC change and has a substantial impact on global/regional climate (Cai et al.

✉ Shahriar Abdullah
shahriar3a@gmail.com

Sk. Md. Abubakar Abdullah
sma.abdullah@gmx.com

Yasin Wahid Rabby
yasinwr@wfu.edu

[1] Department of Environmental Science and Disaster Management, Noakhali Science and Technology University, Noakhali 3814, Bangladesh

[2] Department of Earth Sciences, University of Hamburg, Hamburg, Germany

[3] Department of Engineering, Wake Forest University, Winston-Salem, NC, USA

2018; Peng et al. 2018; Wang et al. 2019; Karakuş 2019). It is also a critical variable for regulating surface energy balance (He et al. 2019). Though both air and land surface temperature (LST) are influenced by a number of factors, non-evaporative surfaces such as urban infrastructures, road, factories, buildings or any type of construction and dry surfaces significantly influence LST (Kayet et al. 2016; El-Zeiny and Effat 2017; Sannigrahi et al. 2018). Thus, LST is a major input to examine surface urban heat island (SUHI) (Chakraborty and Lee 2019), resulting from large-scale modification of land use/cover (Dewan et al. 2021). This kind of situation is pervasive in unplanned metropolis with insufficient amount of greenery and water bodies. Hence, it is well understood that LST estimation and identifying its relationship with LULC can be an effective tool for evaluating environmental conditions, inhabitability and sustainability of any region.

Both in-situ and remotely sensed data are used for LST and LULC mapping. However, in-situ data collection is costly, and unavailability of historical records can be a big obstacle. Moreover, mapping land cover type of a large region is difficult to carry out with field survey. Remotely sensed data are shown to overcome this obstacle. Recently, various satellite sensors like moderate resolution imaging spectroradiometer (MODIS), advanced very high-resolution radiometer (AVHRR), thematic mapper (TM), enhanced thematic mapper plus (ETM+), operational land imager/thermal infrared sensor (OLI/TIRS) are used in LST and LULC mapping (Cristóbal et al. 2018; Shi and Zhang 2018; Xue et al. 2019). Among them, Landsat TM, ETM+ and OLI/TIRS are particularly useful due to their high resolution (compared with MODIS or AVHRR) and long-term data availability (Shi and Zhang 2018; Soydan 2020).

The relationship between LULC and LST can be explored by two approaches (Zhou and Wang 2011). First, by associating LST with LULC (Voogt and Oke 2003). Second, by establishing the relationship with different biophysical variables such as normalized difference vegetation index (NDVI) (Rouse et al. 1974), normalized difference built-up index (NDBI) (Zha et al. 2003), modified normalized difference water index (MNDWI) (Xu 2006) and bare soil index (BSI) (Rikimaru et al. 2002) with LST. Some studies have used both techniques to provide evidence of increasing LST as a result of land use/cover change (Dewan and Corner 2012; Trotter et al. 2017; Das and Angadi 2020; Tariq et al. 2020).

Though many works have illustrated the relationship between LULC and LST on different cities of Bangladesh including Chittagong city corporation area (Chaudhuri and Mishra 2016; Trotter et al. 2017; Dewan et al. 2021; Raja et al. 2021; Roy et al. 2021; Gazi et al. 2021), study utilizing multi-seasonal data is lacking. For example, most of the existing works on LST in Bangladeshi cities have dealt with a single month temperature to represent entire year (Chaudhuri and Mishra 2016; Raja et al. 2021). However, a clear and accurate representation of the whole year requires LST computation for different seasons. Also, most of the previous works have used maximum likelihood method for classification (Dewan and Yamaguchi 2009; Chaudhuri and Mishra 2016). Few, however, have used support vector machine (SVM) method, but there is no work that has used advanced artificial neural network (ANN) algorithm for LULC classification. In addition, recent studies have showed that the intensity of SUHI has become a common feature for Chittagong area with marked seasonal variations, resulting in the narrowing of diurnal temperature range (DTR) (Dewan et al. 2021). On the other hand, attributes such as population density, elevation, slope, aspect, road networks, etc. have been used to forecast LST but studies examining the association between biophysical variables and LST is few and far between.

In this study, we have addressed a research gap by detailing the impact of LULC change on land surface temperature in Chittagong Metropolitan Area (CMA). We extended our work by modeling the impact of land cover change on LST for 2050.

2 Study Area

The CMA is located between latitude 22° 6′ to 22° 3′ and longitude 91° 41′ to 92° 3′, and is bounded by the Bay of Bengal on the west, the Karnafuli River on the southwest, the Halda River on the northeast, and Rangamati district on the east (Fig. 1). It is the second largest metropolitan area of Bangladesh with a population of around 8 million people within an area of 715.16 km^2 (BBS 2011). Population, which is a major factor behind rapid urban expansion, is increasing in a substantial manner due to widespread employment opportunities. Apart from population increase, urbanization is driven by economic development, commercialization, and modernization (Roy et al. 2020).

Geographically, CMA is a coastal hilly region, and the hills on the southeastern portion are known as the Chittagong Hill Tracts (CHT). Climatologically, CMA has hot summer (April to June) and relatively cold winter (November to February) due to tropical monsoon climate (Adnan et al. 2019). The maximum temperature recorded by Bangladesh Meteorological Department (BMD) is 38.9 °C in April and the lowest is 5.2 °C in January, but the average temperate remains between 24 and 28 °C (BBS 2011). Annual precipitation ranges from

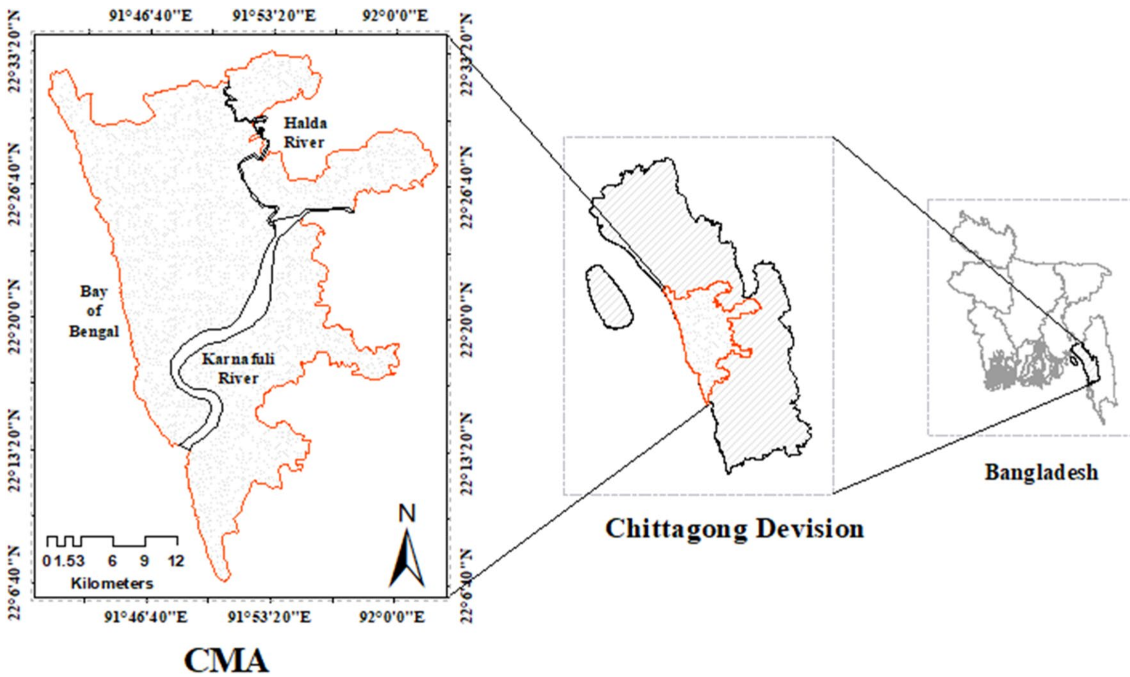

Fig. 1 Location of the study area

2400 to 3000 mm. Chittagong is also known as the economic capital of Bangladesh and the center of all business and economic activities. It had been an important seaport of the South Asian region since the ninth century. The area is also full of natural resources, especially forest resources. However, CMA is prone to a range of disasters, including cyclones, landslides, and earthquakes (Islam et al. 2017). Also, the area is certainly missing sustainable planning aspect regarding its geographical location. Therefore, continuous monitoring of its climate and land change pattern is important for future planning of the city, and to tackle any uncertain catastrophic activities in the economic hub of Bangladesh.

3 Materials and Methods

3.1 Data and Image Pre-processing

A total of 18 images from Landsat 5 TM (1990 and 2005) and Landsat 8 OLI/TIRS (2020) sensors were acquired for three different seasons (summer, winter and autumn) from USGS (Landsat 7 Data Users Handbook 2019; Landsat 8 Data Users Handbook 2019). They were from path 136/44 and 136/45, which were then mosaiced. The data (Level 1 Terrain Corrected) were geo-referenced to UTM zone 45 (Table 1).

Table 1 Attributes of Landsat data used in this study

Acquisition date	Season	Satellite	Sensor	Resolution (m)	Data used for			Source
					LULC	LST	Bio-physical indices	
16 January 1990	Winter	Landsat 5	TM	30/120	✓	✓	✓	USGS
06 April 1990	Summer				X	✓	✓	
9 July 1990	Autumn				X	✓	✓	
25 January 2005	Winter	Landsat 5	TM	30/120	✓	✓	✓	
15 April 2005	Summer				X	✓	✓	
20 July 2005	Autumn				X	✓	✓	
1 January 2020	Winter	Landsat 8	OLI/TIRS	30/100	✓	✓	✓	
24 April 2020	Summer				X	✓	✓	
11 July 2020	Autumn				X	✓	✓	

Using the fast line-of-sight atmospheric analysis of spectral hypercubes (FLAASH) algorithm, atmospheric correction was done.

3.2 Methods

3.2.1 LULC Classification

Among the three seasons, images of winter for all respective years were used for LULC analysis, as the sky remains relatively clear during winter. The images were classified using ANN algorithm for its high accuracy in ENVI (Environment for Visualizing Images) software. This is a non-parametric supervised classifier which uses back-propagation learning algorithm and consists of three layers; i.e., input, hidden and output layer. During the image classification, neurons in input layer denote image bands, whereas output layer neurons represent LULC features (Srivastava et al. 2012). The network error is minimized by back-propagation till the neural network can generate continuous input–output relations with a certain level of accuracy (Gopal and Woodcock 1996). The hidden layer's learning rate was set to 100, while output layer's was set to 0.01 with a 0.001 stopping criteria. However, false color composition (FCC) was created via reflective bands of Landsat and collected 250 training samples for 5 different land features (vegetation, agriculture, water bodies, bare land and built-up) to train the model. The function of ANN can be expressed with the following equation:

$$o_j = 1\big/\left(1 + e^{-\lambda \mathrm{net}_j}\right) \tag{1}$$

where O_j is the output of external input j and λ is a gain factor. The term net_j can be computed by (Schalkoff 1997):

$$\mathrm{net}_j = \sum_i w_{ji} o_i \tag{2}$$

where w_{ji} is the weight of interconnection channel to unit j, from unit i and o is the output of external unit i.

3.2.2 Accuracy Assessment

The best method to collect sample data for accuracy assessment is field survey. But rapid land use changes often make field work challenging. Therefore, usage of satellite images as the source of reference is also accepted in the scientific community. The most frequently used validation tool for land cover classified maps is kappa statistics (Cohenx 1960), as it gives significantly precise results than other validation methods (Foody 1992). It ranges from 0 to 1, with 0 denoting poor agreement and 1 representing nearly perfect agreement. Also, accuracy of each LULC class can be quantified by applying user's and producer's accuracy (Story and Congalton 1986). However, in our study, the accuracy of a LULC classification was calculated by developing a confusion or error matrix with 500 sample sites which compared the classified LULC maps with reference data. The kappa coefficient (K), overall accuracy (OA), user's accuracy (UA), and producer's accuracy (PA) were then derived from this error matrix.

3.3 Extraction of LST

To understand the effect of LULC changes and urbanization on temperature, LST is used. It has also a direct relation with the biophysical components. There are a number of algorithms available to compute LST from Landsat data, however, mono window algorithms (MWA) (Qin et al. 2001) and single channel algorithms (SCA) (Jiménez-Muñoz and Sobrino 2003) require water vapor data which was not available for our study area. Alternatively, we have used an image-based method developed by USGS to calculate LST from Landsat images (USGS 2016). Band 6 and band 10 of TM and TIRS data were used to retrieve LST using the following steps:

Step 1 Transformation of digital number (DN) to spectral radiance (L_λ)

Every object emits electromagnetic energy as the object temperature is greater than 0 (zero) Kelvin (K) or absolute 0 (zero). Thermal sensor collects signals and can transform to sensor radiance. For TIRS (Landsat 8), spectral radiance estimation (L_λ) was performed using the following formula (Landsat 8 Data Users Handbook 2019):

$$L_\lambda = M_\mathrm{L} * Q_\mathrm{CAL} + A_\mathrm{L} \tag{3}$$

where L_λ is the sensor spectral radiance, M_L is the band's radiance multiplicative scaling factor, A_L is the band's radiance additive scaling factor, Q_CAL is Quantized and calibrated radiance value. For TM/ETM + (Landsat 4,5/7), the spectral radiance required the following formula (Landsat 7 Data Users Handbook 2019):

$$L_\lambda = L_{\min\lambda}\left[\left(L_{\max\lambda} - L_{\min\lambda}\right)\big/\left(Q_{\mathrm{CAL}_{\max}} - Q_{\mathrm{CAL}_{\min}}\right)\right] * Q_\mathrm{CAL} \tag{4}$$

where $L_{\max\lambda}$ and $L_{\min\lambda}$ are the maximum and minimum spectral radiance ($\mathrm{Wm^{-2}sr^{-1}\,\mu m^{-1}}$). $Q_{\mathrm{CAL}_{\max}}$ is the maximum DN value of the image and $Q_{\mathrm{CAL}_{\min}}$ is the minimum DN value of the image, here 255.

Step 2 Transformation of spectral radiance (L_λ) to brightness temperature (BT)

It is important to convert spectral radiance (L_λ) to brightness temperature (BT). The following theorem measures BT in °C (Landsat 7 Data Users Handbook 2019; Landsat 8 Data Users Handbook 2019):

$$\mathrm{BT} = \left[K2/\left(\ln\left(K1/L_\lambda\right)+1\right)\right] - 273.15 \quad (5)$$

The value for $K1$ and $K2$ can be retrieved from respective metadata file.

Step 3 Estimating land surface emissivity

Land surface emissivity is considered as a proportionality factor of Plank's Law. This can be calculated as (Sobrino et al. 2004):

$$\epsilon = 0.004Pv + 0.986 \quad (6)$$

where ϵ is the land surface emissivity and P_v is the proportion of vegetation.

$$P_v = \left[\left(\mathrm{NDVI} - \mathrm{NDVI}_{\min}\right)/(\mathrm{NDVI}_{\max} - \mathrm{NDVI}_{\min})\right]^2 \quad (7)$$

where $\mathrm{NDVI}_{\max}$ is the maximum value of NDVI and $\mathrm{NDVI}_{\min}$ is the minimum.

Step 4 Estimating LST

This is the final stage of calculating LST. This can be computed as:

$$\mathrm{LST} = \mathrm{BT}/[1 + ((\lambda \mathrm{BT}\sigma/hc) * \ln \epsilon)] \quad (8)$$

where BT is the brightness temperature, λ is the spectral radiance, h is the Plank's Constant ($6.626 \times 10-34$ J K^{-1}), c is the velocity of light (2.998×108 m s^{-1}) and σ is the Boltzmann constant ($1.38 \times 10-23$ J K^{-1}). While comparing LST from different time periods, especially when comparing seasonal variation of LST, it is recommended to normalize or standardizee LST values (Carlson and Traci Arthur 2000; Trotter et al. 2017). Thus, our LST values were normalized.

3.4 Extraction of Biophysical Parameters

A few biophysical indices were calculated for a better perception of the change of a specific land cover. The relationship between these indices and LST were also studied to understand the impact on LST. Nevertheless, NDVI (Rouse et al. 1974), NDBI (Zha et al. 2003), MNDWI (Xu 2006) and BSI (Rikimaru et al. 2002), which respectively, indicate greenness or vegetation, built-up or impervious surfaces, open water bodies and soil without grass or any object of any area, were calculated using the following formulas.

$$\mathrm{NDVI} = \left(B_{\mathrm{NIR}} - B_{\mathrm{R}}\right)/(B_{\mathrm{NIR}} + B_{\mathrm{R}}) \quad (9)$$

$$\mathrm{NDBI} = \left(B_{\mathrm{SWIR1}} - B_{\mathrm{NIR}}\right)/\left(B_{\mathrm{SWIR1}} + B_{\mathrm{NIR}}\right) \quad (10)$$

$$\mathrm{MNDWI} = \left(B_{\mathrm{G}} - B_{\mathrm{MIR}}\right)/\left(B_{\mathrm{G}} + B_{\mathrm{MIR}}\right) \quad (11)$$

$$\mathrm{BSI} = [((B_{\mathrm{SWIR1}} + B_{\mathrm{R}}) - (B_{\mathrm{NIR}} + B_{\mathrm{B}}))/((B_{\mathrm{SWIR1}} + B_{\mathrm{R}}) + (B_{\mathrm{NIR}} + B_{\mathrm{B}}))] + 1 \quad (12)$$

where NIR is near-infrared (TM band 4 and OLI band 5), R is red band (TM band 3 and OLI band 4), SWIR1 is shortwave infrared1 (TM band 5 and OLI band 6), G indicates green band (TM band 2 and OLI band 3) and B is blue band (TM band 1 and OLI band 2).

3.5 Predicting LST

To ascertain long-term impact of LULC change on LST, it is useful to predict future scenario of LST under current LULC change. There are several methods such as artificial neural network (ANN), regression model and hybrid neural models, which are applied in various studies (Corner et al. 2014; Ghosh et al. 2019; Nurwanda and Honjo 2020). In this work, we have used ANN method to predict the LST for the year 2050, which is regarded as an effective method in predicting with preceding data (Mas and Flores 2008; Ullah et al. 2019; Al Kafy et al. 2021). A Multi-layer Feed forward back Propagation ANN method in MATLAB software was adopted to forecast LST for the year 2050. The Multi-Layer Perceptron (MLP) neural network uses autonomous calculations about how to adjust provided parameters for a better output. However, when ANN algorithm reads the patterns, it generates a random output with poor accuracy and then computes the difference between low accurate output and the desired output. The iterative cycle repeats until the network output meets the target output with an acceptable error (Silva and Clarke 2002; Ullah et al. 2019).

During model training, biophysical variables (NDVI, NDBI, MNDWI, and BSI), classified images, latitude and longitude were employed as input variables and retrieved LST data as output. The initial learning rate (μ) was set to 0.1, and the decay rate (β) was used to regulate it. The pixel values for all images were also converted to continuous data to improve the performance. Apart from network creation, training, and prediction, our prediction model also incorporates performance evaluation. Mean Square Error (MSE) and correlation coefficient (R) were used to measure reliability of the network.

4 Results and Discussion

4.1 LULC Change Detection

The spatial pattern of LULC for the years 1990, 2005 and 2020 is shown in Fig. 2. In both 1990 and 2005, vegetation was prevalent followed by bare land, agriculture, waterbodies and built-up in 1990 and bare land, agriculture, built-up and waterbodies in 2005 (Table 2). But in 2020, agricultural land has surpassed vegetation and was seen to cover almost 39% of the study area.

As a result of excessive destruction of vegetative areas for development purpose, it has lost 10,447.51 hectares (ha) of land in the last 30 years. Bare lands have also dramatically decreased from 20,342.3 ha to 2695.6 ha from 1990 to 2020. Built-up areas and waterbodies on the other hand have increased in this 3 decades. With a maximum change rate (4.6%), built-up area has reached 17.5% of CMA in 2020 from 3.1% in 1990, and waterbodies has almost doubled between 1990 and 2020.

From Fig. 2, it can be noticed that most of the vegetation patches that were available in 1990 started disappearing in 2005 and were transformed to other LULC in 2020. Only a noticeable patch can be identified in the northern side of the city, which is basically a hilly region. Eastern and north-eastern parts also have some small patches which may also disappear soon, if present trend of land cover change continues. Again, most of the bare lands near the river or city center have turned into built-up areas and some have turned into agricultural lands in both 2005 and 2020. The city has expanded from the riverbank mainly to northern part and a small portion to southern part of CMA. However, rapid population rise is mainly responsible for this unplanned and unsustainable land cover change. In fact, to meet the need for housing and food of the growing population, vegetation and bare land have converted to either built-up or agricultural lands, and this changing trend is common in developing countries around the world, including Bangladesh (Mishra and Rai 2016; Pawe and Saikia 2018; Hatab et al. 2019; Astuti et al. 2019; Roy et al. 2021; Gazi et al. 2021).

4.2 Accuracy Assessment

Accuracy of land cover classification has showed an overall accuracy of our classified data as 86.40%, 87.20% and 88.00%, respectively, for the years 1990, 2005 and 2020. The

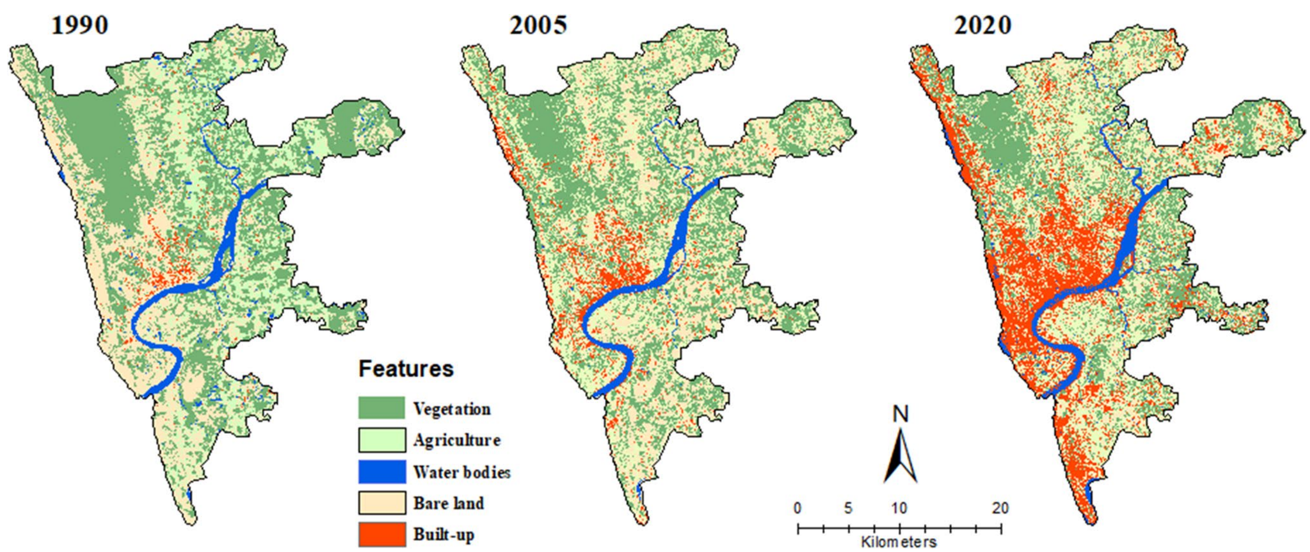

Fig. 2 LULC map of CMA in 1990, 2005 and 2020

Table 2 Area and percent of LULC covers in CMA

LULC type	1990		2005		2020		Change rate 1990–2020
	Area (ha)	%	Area (ha)	%	Area (ha)	%	
Vegetation	30,434.89	42.56	25,325.58	35.41	19,987.38	27.94	− 0.34327
Agriculture	14,343.95	20.06	15,542.85	21.73	27,862.14	38.96	0.94243
Waterbodies	4147.56	5.80	6352.96	8.88	8458.43	11.83	1.03937
Bare land	20,342.27	28.44	16,761.58	23.44	2695.55	3.77	− 0.86749
Built-up	2247.22	3.14	7532.92	10.53	12,512.39	17.50	4.56794

kappa coefficient was 0.83 in 1990, 0.84 in 2005 and 0.85 in 2020. Thus, it can be said that the accuracy of our classified images has satisfied accuracy metric. The detailed result of accuracy assessment is shown in Table 3.

4.3 Changing Trend of LST

Surface temperature of 1990, 2005 and 2020 for the winter, summer and autumn seasons were extracted. In the winter season, the lowest temperature of 1990 was 14.05 °C where the highest was 23.26 °C in 2005, the highest temperatures increased to almost 2 °C where the lowest was almost the same as 1990. But in 2020, both the highest and the lowest temperatures increased in noticeable manner, which ranges between 15.75 and 29.46 °C (Table 4). In the summer season, a slight decrease in the lowest temperature was seen in 2005 (25.16 °C) from 1990 (26.59 °C). This might not be the same for the whole season as our study has analyzed single day temperature. However, the highest temperature was 32.81 °C in 1990, 33.21 °C in 2005 and 36.53 °C in 2020. In the autumn season, lowest temperatures were almost the same for all the three years, but the highest temperature has gradually increased and ended up at 29.61 °C in 2020, which was 26.13 °C in 1990. The average temperature has increased almost 2.5 °C between 1990 and 2020 (Table 4). Overall, average temperature has increased by almost 2 °C in the last 30 years. Other studies also reported a rise of temperature in the study area (Roy et al. 2020; Dewan et al. 2021; Raja et al. 2021).

Table 4 Descriptive statistics of LST

Year	Season	Min	Max	Seasonal average	Yearly average
	Winter	14.05	23.26	18.65	
1990	Summer	26.59	32.81	29.7	24.32
	Autumn	23.11	26.13	24.62	
	Winter	14.56	25.63	20.09	
2005	Summer	25.16	33.21	29.18	24.84
	Autumn	22.93	27.58	25.25	
	Winter	15.75	29.46	22.61	
2020	Summer	26.21	36.53	31.37	26.70
	Autumn	22.52	29.61	26.07	

Table 3 Accuracy assessment of LULC classification

Year	Land cover	Vegetation	Agriculture	Waterbodies	Bare land	Built-up	Total	User's accuracy	Kappa coefficient
2020	Vegetation	40	4	2	0	1	47	85.11	0.85
	Agriculture	3	45	1	0	2	51	88.24	
	Waterbodies	1	1	41	1	0	44	93.18	
	Bare land	4	1	0	48	0	53	90.57	
	Built-up	0	5	2	2	46	55	83.64	
	Total	48	56	46	51	49	250		
	Producer's Accuracy	83.33	80.36	89.13	94.12	93.88			
	Overall accuracy		88.00						
2005	Vegetation	45	5	1	2	0	53	84.91	
	Agriculture	4	43	2	3	1	53	81.13	
	Waterbodies	1	2	42	0	0	45	93.33	0.84
	Bare land	1	3	0	46	1	51	90.20	
	Built-up	2	0	1	3	42	48	87.50	
	Total	53	53	46	54	44	250		
	Producer's accuracy	84.91	81.13	91.30	85.19	95.45			
	Overall accuracy		87.20						
1990	Vegetation	35	3	3	1	0	42	83.33	
	Agriculture	5	41	2	0	2	50	82	
	Waterbodies	2	0	41	1	4	48	85.42	0.83
	Bare land	1	2	0	48	2	53	90.57	
	Built-up	0	1	3	2	51	57	89.47	
	Total	43	47	49	52	59	250		
	Producer's accuracy	81.4	87.23	83.67	92.31	86.44			
	Overall accuracy		86.4						

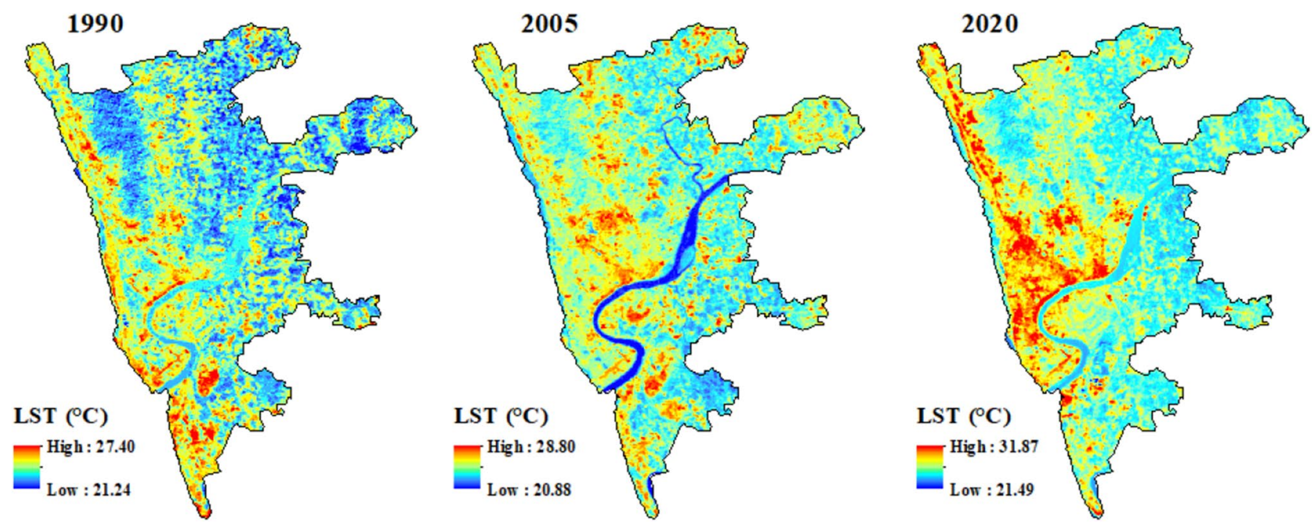

Fig. 3 Spatiotemporal distribution of LST

Fig. 4 LST according to land cover categories: **a** 1990, **b** 2005 and **c** 2020

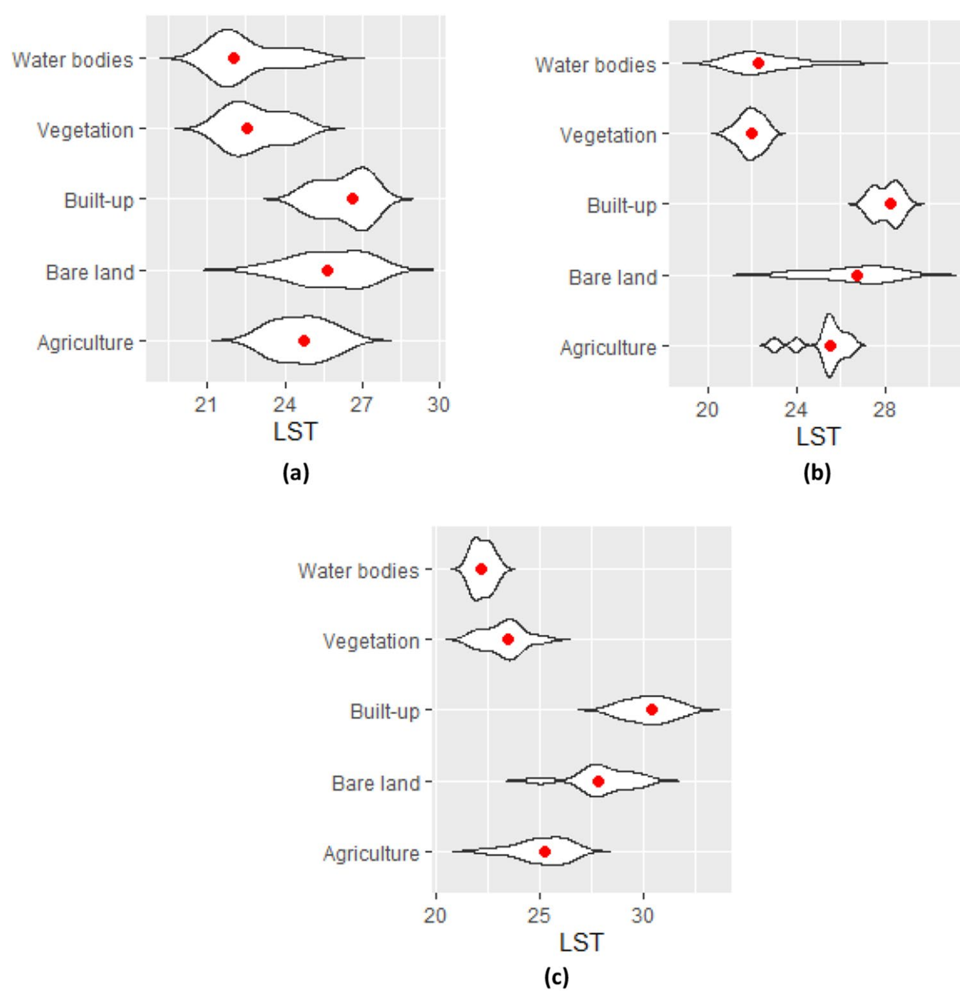

The spatially distributed average temperature for the years 1990 and 2020 is displayed in Fig. 3.

4.4 Relationship Between LST and LULC

Figure 4 shows the range and density of temperature distribution of each land cover type. The average temperature of each class is indicated by a red dot. It can be seen that, in every class in every year, density is always high around the point of average temperature, indicating that the temperature of each class covers the majority of CMA. On the other hand, high and low temperature values of each class have very low density; thus, comprising very few numbers of pixels and covering a small portion of the study area.

LST varies from one type of land cover to another type based on emission property of land features (Voogt and Oke 2003). The non-evaporative surfaces like built-up and bare lands exhibit more temperature than evaporative surfaces like waterbodies and vegetations. Correspondingly, in this work, bare lands and built-up have showed higher temperature range, whereas waterbodies, vegetation and agriculture have showed lower or moderate temperature range (Fig. 4). The average temperature of built-up and bare land had increased noticeably between 1990 and 2020. From 26.8 °C in 1990, average temperature of built-up has increased to 28.2 °C in 2005 and 31.2 °C in 2020. The average temperature of bare land had also increased to 27.6 °C in 2020 from 25.6 °C in 1990. On the other hand, vegetation and agricultural lands have showed, respectively, an average temperature of 22.5 °C and 24.8 °C in 1990, 22 °C and 25.7 °C in 2005 and 22.9 °C and 25.1 °C in 2020. However, average temperature of water bodies was almost the same for all three years. This indicates not only that built-up and bare land encompass higher temperature range but also the consistent increase in intensity of temperature in these features; conversely, features such as vegetation, waterbodies and agricultural lands keep the temperature low and almost constant.

According to Fig. 3, most of the high-temperature zones in 1990 were in the western part of the city, with some in the center. Because of the availability of water, industries and factories developed along the riverbank, high-temperature zones along the river are mostly caused by the heat generated and emitted by those industries. The northern part of the city showed lower temperature as most of the parts in the north are hilly regions. The eastern part of the city is basically the transition zone between urban and rural areas. Vegetation was also abundant in that part of CMA; thus, temperature was low. But, in 2005 and 2020, high to mid-range temperature zone engulfed almost the whole city as a result of unplanned and uncontrolled urbanization. Destruction of the vegetative cover in the northern and eastern part, which are mostly replaced by built-up area and agricultural lands, also had a significant impact on the temperature rise.

4.5 Relationship Between LST and Biophysical Components

Each biophysical index was measured for all the three seasons and averaged for that year. To identify the relationship between LST and biophysical indices, individual regression analysis was performed in the statistical software R (Figs. 5, 6, 7, 8). Furthermore, correlation between LST and NDVI, NDBI, MNDWI and BSI was also calculated for each year Fig. 9.

Figure 5 shows the slope between NDVI and LST to be downwards for both the years, which indicates that NDVI and LST are negatively correlated (− 0.78 in 1990, − 0.27 in 2005 and − 0.35 in 2020). MNDWI also shows a negative correlation (− 0.25 in 1990, − 0.16 in 2005 and − 0.43 in 2020) with LST as in Fig. 6.

Conversely, the slope of NDBI and BSI has showed an upward trend. The correlation value between LST and NDBI was 0.65, 0.48 and 0.62 in 1990, 2005 and 2020, respectively (Fig. 7). This indicates that the intensity of built-up areas or impervious surfaces is directly related to the temperature rise. The scenario is similar for BSI where the correlation between LST and BSI was 0.44, 0.11 and 0.31 in 1990, 2005 and 2020, respectively (Fig. 8). This is because the non-evaporative surfaces cannot release their latent heat through evaporation or evapotranspiration, and surface absorbs or reflects the energy from the Sun; exhibiting high temperature as a result.

However, a clear picture of the relationship between LST and NDVI, NDBI, NDWI, MNDWI and BSI is depicted in Fig. 9. In 1990, the highest correlation was seen between LST and NDBI (0.65), and the lowest between LST and NDVI (− 0.78). A significant positive correlation was also witnessed between LST and BSI (0.44); and a negative correlation between NDVI and NDBI (− 0.59), NDVI and BSI (− 0.43). In 2005, NDBI and BSI also showed the highest correlation (0.56) and BSI and MNDWI showed the lowest correlation (− 0.66). A significant positive correlation was seen between LST and NDBI (0.48) where significant negative correlation was seen between NDVI and MNDWI (− 0.47), NDBI and MNDWI (− 0.53). Again, in 2020, the highest positive correlation was seen between LST and NDBI (0.62). Moreover, NDVI and BSI (0.36), NDBI and BSI (0.39) have also showed significant positive correlation. Conversely, the lowest correlation was seen between MNDWI and BSI (− 0.85), where LST and NDVI (− 0.35), NDVI and NDBI (− 0.58), LST and MNDWI (− 0.43), NDVI and MNDWI (− 0.48) also showed strong negative correlation.

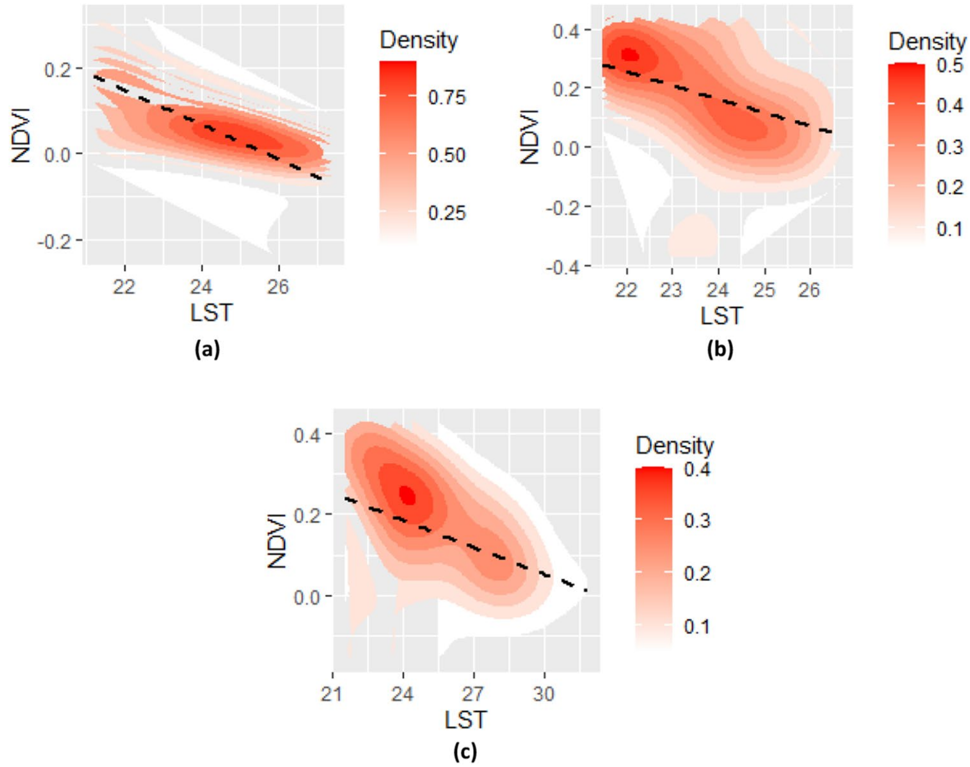

Fig. 5 Correlations between LST and NDVI: **a** 1990, **b** 2005 and **c** 2020

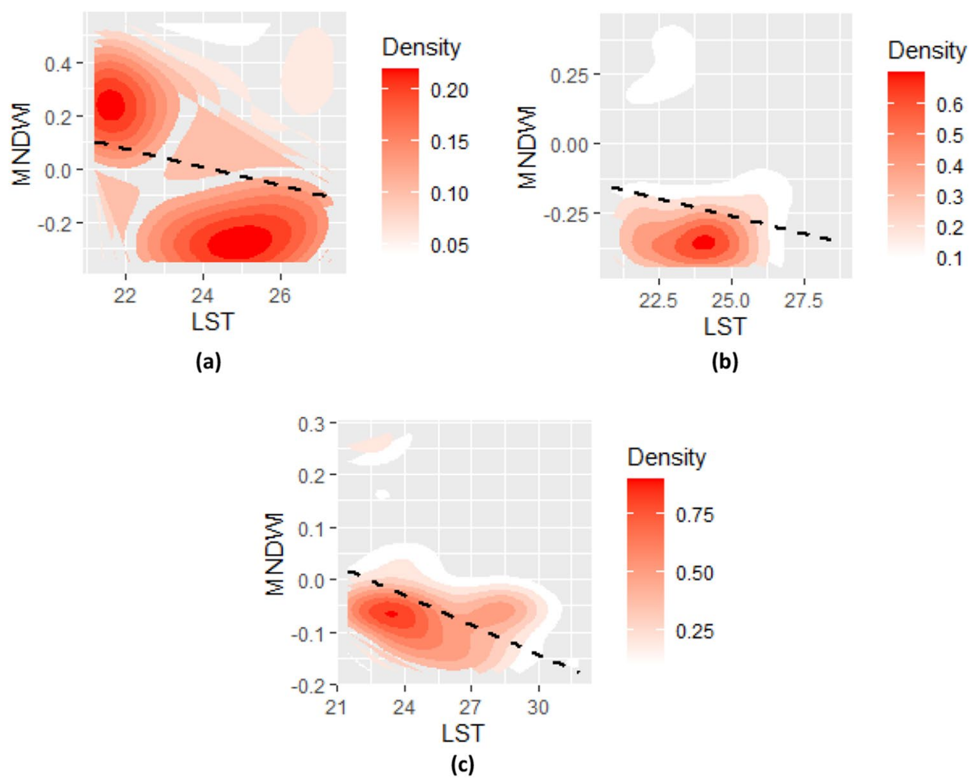

Fig. 6 Correlations between LST and MNDWI: **a** 1990, **b** 2005 and **c** 2020

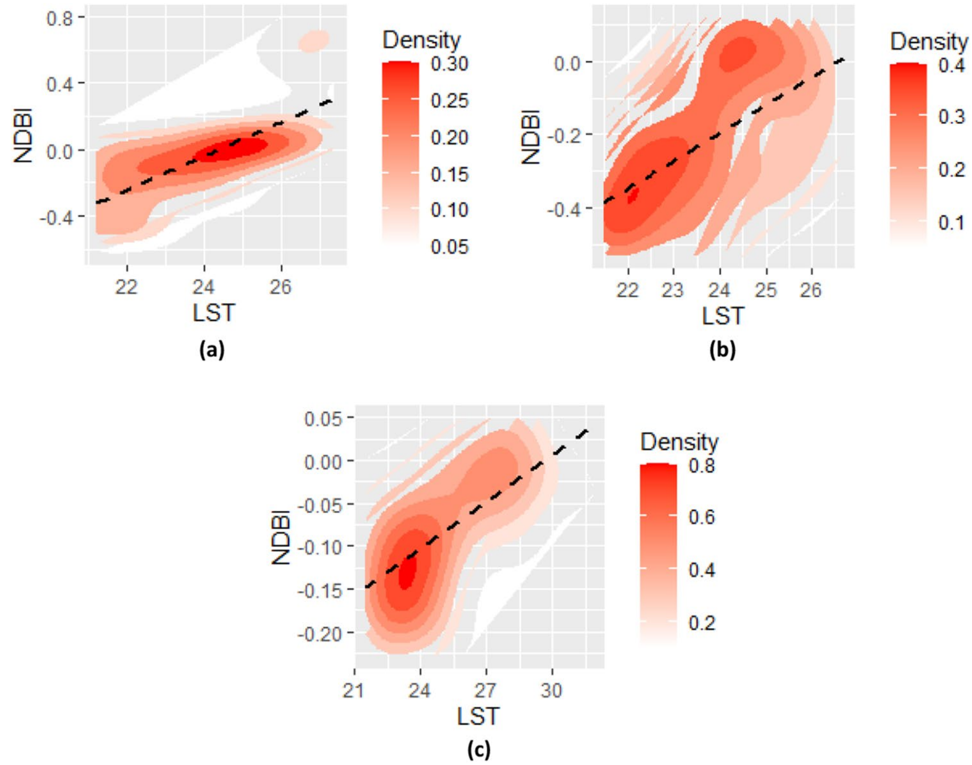

Fig. 7 Correlations between LST and NDBI: **a** 1990, **b** 2005 and **c** 2020

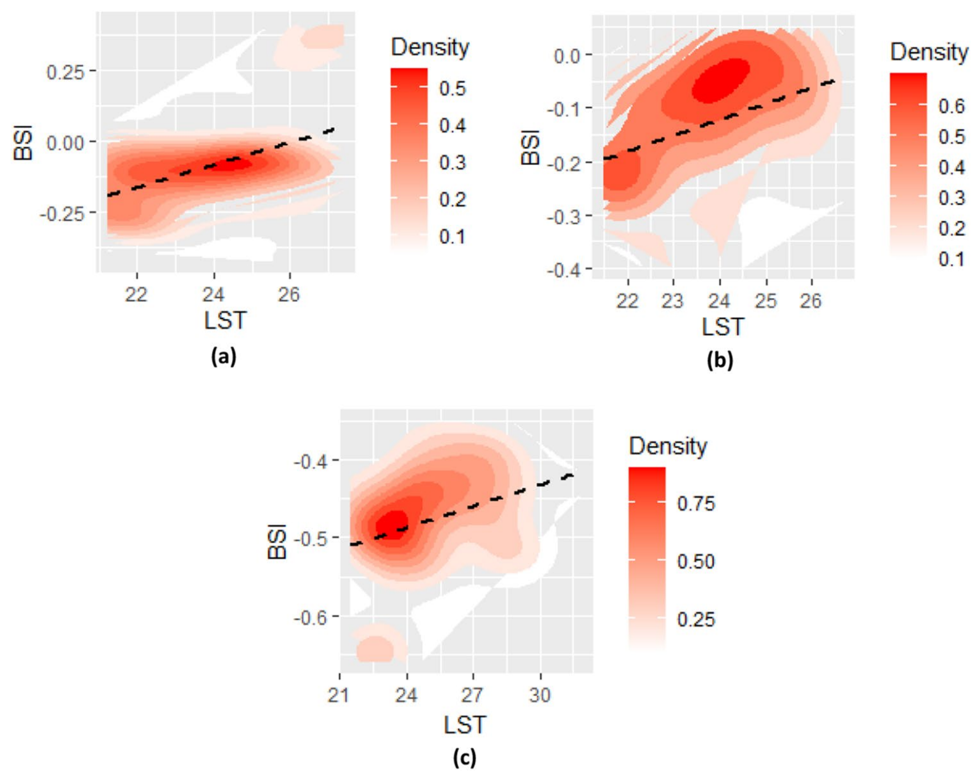

Fig. 8 Correlations between LST and BSI: **a** 1990, **b** 2005 and **c** 2020

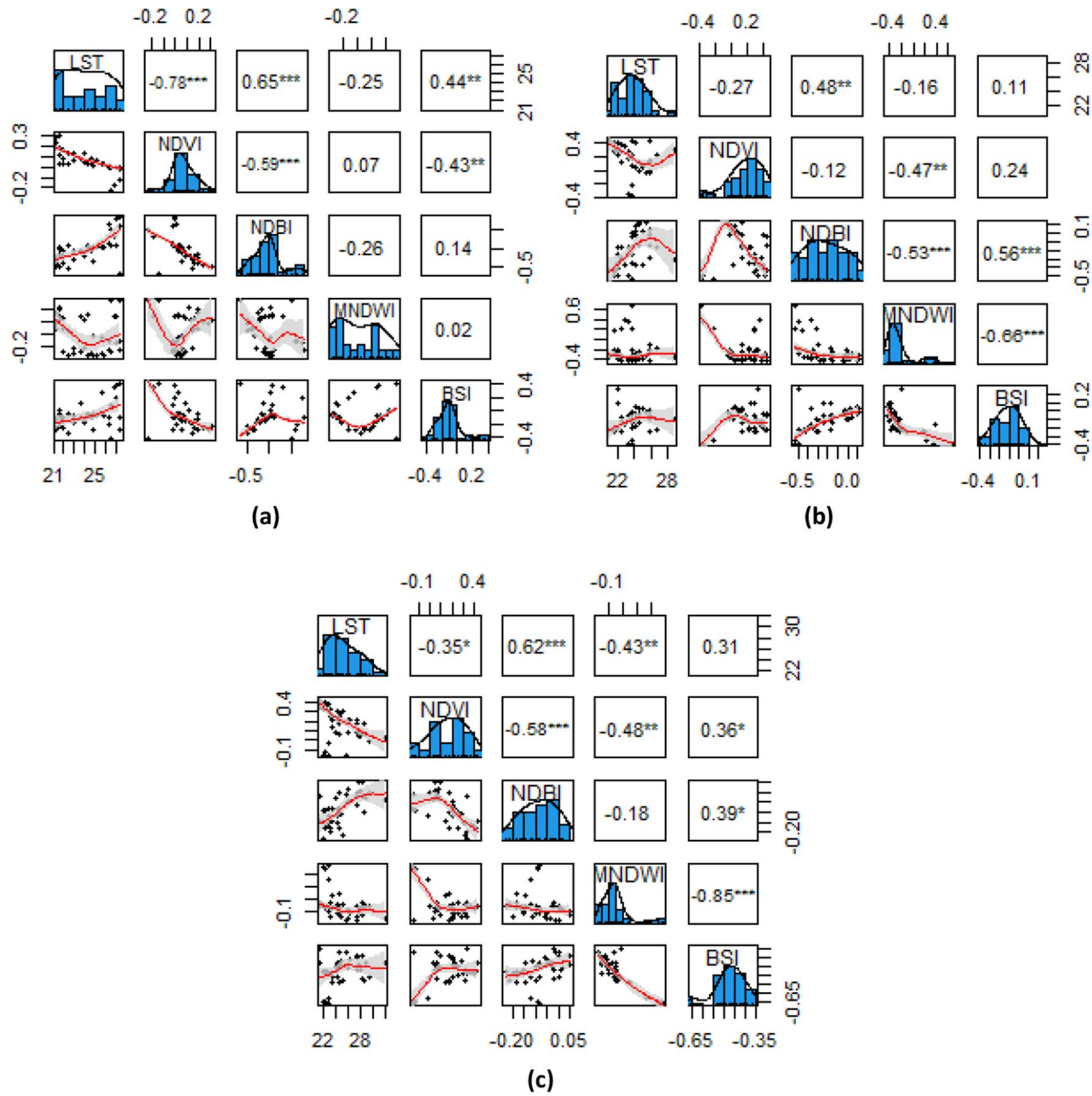

Fig. 9 Correlation between LST and NDVI, NDBI, MNDWI, and BSI: **a** 1990, **b** 2005 and **c** 2020

4.6 Predicting LST for 2050

With the help of ANN, this work has predicted the LST for 2050 (Fig. 10). The MSE and R were 0.56 and 0.82, respectively, indicating a strong positive correlation between the predicted and estimated LST for CMA. It can be seen that the average temperature will rise to 28.04 °C in 2050 from 26.70 °C in 2020. Except for some areas in the eastern and northern part of CMA, where most of the lands are covered with vegetation, water bodies or agriculture, the whole city exhibited high temperature. The temperature is most intense not only over the previous built-up areas but also over its surroundings. This can be an indication that the built-up areas may encompass majority of the areas within 2050.

5 Conclusions

In this study, we have estimated land cover and land surface temperature of CMA for the years 1990, 2005 and 2020 using Landsat TM and OLI/TIRS data and explored the relationship between LULC and LST. Result has revealed that the most of the infrastructural development took place near the Karnafuli river, and LST is high in this region. Conversely, area with vegetation, especially northern hilly region, and water bodies showed low temperature. Moreover, we have measured correlation between temperature and four biophysical indices, i.e., NDVI, NDBI, MNDWI and BSI, to obtain more clear understanding on the influence of land cover change on temperature, and it was found that NDVI and MNDWI are negatively correlated with LST, whereas

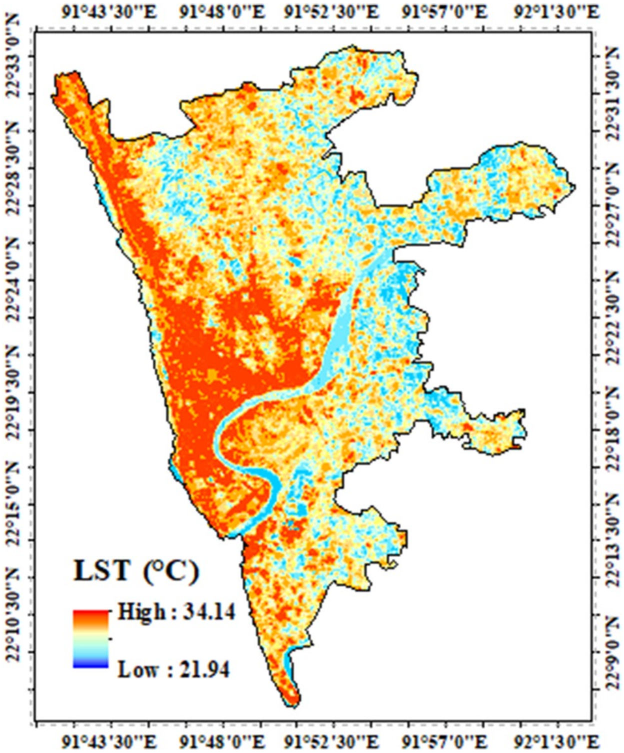

Fig. 10 Predicted temperature (°C) for the year 2050

NDBI and BSI are positively correlated. Finally, to perceive the long-term impact of LULC on LST, we have predicted the temperature of CMA with an ANN model for 2050; the outcome was alarming. Almost the whole area is predicted to exhibit higher temperatures except for some small patches on northern and eastern part of CMA.

The current urbanization pattern of CMA is unplanned and unsustainable, which is already affecting the environment in several ways including rise of LST. Although, the temperature is still in a tolerable limit, according to our prediction, it will rise tremendously by 2050. Therefore, immediate measures should be taken to obstruct the current trend of land cover change by establishing a strong and sustainable city plan. It is also important to promote public awareness so that inhabitants do not destroy natural resources like vegetation and refrain from filling up water bodies for agricultural or construction purposes. Finally, CDA (Chittagong Development Authority) and other relevant organizations should come forward with the aim of a sustainable model city and take proper measures accordingly.

Author contributions SA: conceptualization, investigation, supervision, methodology, writing—review and editing. DB: investigation, resources, software, visualization, original draft. SMAA: conceptualization, writing—review and editing. YWR: conceptualization, writing—review and editing.

Funding No funding is received for this work.

Availability of Data and Materials Not applicable.

Code Availability Not applicable.

Declarations

Conflict of Interest The authors declare that there is no conflict of interest.

Ethics Approval This work has not been published in whole or in part elsewhere, not currently being considered for publication in another, and all authors have been personally and actively involved in this work.

Consent to Participate Not applicable.

Consent for Publication Not applicable.

References

Adnan MSG, Dewan A, Zannat KE, Md Abdullah AY (2019) The use of watershed geomorphic data in flash flood susceptibility zoning: a case study of the Karnaphuli and Sangu river basins of Bangladesh. Nat Hazards 99(1):425–448. https://doi.org/10.1007/s11069-019-03749-3

Al Kafy A, Abdullah-Al-Faisal, Al Rakib A, Akter KS, Rahaman ZA, Jahir DMA, Subramanyam G, Michel OO, Bhatt A (2021) The operational role of remote sensing in assessing and predicting land use/land cover and seasonal land surface temperature using machine learning algorithms in Rajshahi, Bangladesh. Appl Geomatics. https://doi.org/10.1007/s12518-021-00390-3

Astuti IS, Sahoo K, Milewski A, Mishra DR (2019) Impact of land use land cover (LULC) change on surface runoff in an increasingly urbanized tropical watershed. Water Resour Manage 33(12):4087–4103. https://doi.org/10.1007/s11269-019-02320-w

BBS (2011) Bangladesh population and housing census 2011, vol 3. Urban Area Report. Dhaka

Behera MD, Tripathi P, Das P, Srivastava SK, Roy PS, Joshi C, Behera PR, Deka J, Kumar P, Khan ML (2018) Remote sensing based deforestation analysis in Mahanadi and Brahmaputra river basin in India since 1985. J Environ Manage 206:1192–1203. https://doi.org/10.1016/j.jenvman.2017.10.015

Cai M, Ren C, Xu Y, Lau KK-L, Wang R (2018) Investigating the relationship between local climate zone and land surface temperature using an improved WUDAPT methodology—a case study of Yangtze River Delta, China. Urban Clim 24:485–502. https://doi.org/10.1016/j.uclim.2017.05.010

Carlson TN, Traci Arthur S (2000) The impact of land use—land cover changes due to urbanization on surface microclimate and hydrology: a satellite perspective. Glob Planet Change 25(1–2):49–65. https://doi.org/10.1016/S0921-8181(00)00021-7

Chakraborty T, Lee X (2019) A simplified urban-extent algorithm to characterize surface urban heat islands on a global scale and examine vegetation control on their spatiotemporal variability. Int J Appl Earth Obs Geoinf 74:269–280. https://doi.org/10.1016/j.jag.2018.09.015

Chaudhuri G, Mishra NB (2016) Spatio-temporal dynamics of land cover and land surface temperature in Ganges-Brahmaputra delta: a comparative analysis between India and Bangladesh. Appl Geogr 68:68–83. https://doi.org/10.1016/j.apgeog.2016.01.002

Cohenx J (1960) A coefficient of agreement for nominal scales. Educ Psychol Meas 20:37–46

Corner RJ, Dewan AM, Chakma S (2014) Monitoring and prediction of land-use and land-cover (LULC) change. In: Dhaka megacity. Springer, pp 75–97

Cristóbal J, Jiménez-Muñoz JC, Prakash A, Mattar C, Skoković D, Sobrino JA (2018) An improved single-channel method to retrieve land surface temperature from the Landsat-8 thermal band. Remote Sens 10(3):431. https://doi.org/10.3390/rs10030431

Das S, Angadi DP (2020) Land use-land cover (LULC) transformation and its relation with land surface temperature changes: a case study of Barrackpore Subdivision, West Bengal, India. Remote Sens Appl Soc Environ 19:100322. https://doi.org/10.1016/j.rsase.2020.100322

Dewan AM, Corner RJ (2012) The impact of land use and land cover changes on land surface temperature in a rapidly urbanizing megacity. In: 2012 IEEE international geoscience and remote sensing symposium. IEEE, pp 6337–6339

Dewan AM, Corner RJ (2014a) Dhaka megacity: Geospatial perspectives on urbanisation, environment and health. Dhaka Megacity Geospatial Perspect Urban Environ Heal. https://doi.org/10.1007/978-94-007-6735-5

Dewan AM, Yamaguchi Y (2009) Land use and land cover change in Greater Dhaka, Bangladesh: using remote sensing to promote sustainable urbanization. Appl Geogr 29(3):390–401

Dewan A, Kiselev G, Botje D (2021) Diurnal and seasonal trends and associated determinants of surface urban heat islands in large Bangladesh cities. Appl Geogr 135:102533. https://doi.org/10.1016/j.apgeog.2021.102533

Dewan A, Kiselev G, Botje D, Mahmud GI, Bhuian MdH, Hassan QK (2021) Surface urban heat island intensity in five major cities of Bangladesh: Patterns drivers and trends. Sustain Cities Soc. 71: https://doi.org/10.1016/j.scs.2021.102926

El-Zeiny AM, Effat HA (2017) Environmental monitoring of spatiotemporal change in land use/land cover and its impact on land surface temperature in El-Fayoum governorate, Egypt. Remote Sens Appl Soc Environ 8:266–277. https://doi.org/10.1016/j.rsase.2017.10.003

Foody GM (1992) On the compensation for chance agreement in image classification accuracy assessment. Photogramm Eng Remote Sensing 58(10):1459–1460

Gazi MY, Rahman MZ, Uddin MM, Rahman FMA (2021) Spatio-temporal dynamic land cover changes and their impacts on the urban thermal environment in the Chittagong metropolitan area, Bangladesh. GeoJournal 86(5):2119–2134. https://doi.org/10.1007/s10708-020-10178-4

Ghosh S, Das CN, Dinda S (2019) Relation between urban biophysical composition and dynamics of land surface temperature in the Kolkata metropolitan area: a GIS and statistical based analysis for sustainable planning. Model Earth Syst Environ 5(1):307–329. https://doi.org/10.1007/s40808-018-0535-9

Gopal S, Woodcock C (1996) Remote sensing of forest change using artificial neural networks. IEEE Trans Geosci Remote Sens 34(2):398–404. https://doi.org/10.1109/36.485117

Hatab AA, Cavinato MER, Lindemer A, Lagerkvist C-J (2019) Urban sprawl, food security and agricultural systems in developing countries: a systematic review of the literature. Cities 94:129–142. https://doi.org/10.1016/j.cities.2019.06.001

He J, Zhao W, Li A, Wen F, Yu D (2019) The impact of the terrain effect on land surface temperature variation based on Landsat-8 observations in mountainous areas. Int J Remote Sens 40(5–6):1808–1827. https://doi.org/10.1080/01431161.2018.1466082

Hua AK (2017) Land use land cover changes in detection of water quality: a study based on remote sensing and multivariate statistics. J Environ Public Health. https://doi.org/10.1155/2017/7515130

Islam MA, Murshed S, Kabir SMM, Farazi AH, Gazi MY, Jahan I, Akhter SH (2017) Utilization of open source spatial data for landslide susceptibility mapping at Chittagong district of Bangladesh—an appraisal for disaster risk reduction and mitigation approach. Int J Geosci 08(04):577–598. https://doi.org/10.4236/ijg.2017.84031

Jiménez-Muñoz JC, Sobrino JA (2003) A generalized single-channel method for retrieving land surface temperature from remote sensing data. J Geophys Res Atmos. https://doi.org/10.1029/2003JD003480

Karakuş CB (2019) The impact of land use/land cover (LULC) changes on land surface temperature in Sivas City Center and its surroundings and assessment of Urban Heat Island. Asia-Pacific J Atmos Sci 55(4):669–684. https://doi.org/10.1007/s13143-019-00109-w

Kayet N, Pathak K, Chakrabarty A, Sahoo S (2016) Spatial impact of land use/land cover change on surface temperature distribution in Saranda Forest, Jharkhand. Model Earth Syst Environ 2(3):1–10. https://doi.org/10.1007/s40808-016-0159-x

Landsat 7 Data Users Handbook (2019) Landsat Project Science Ofce at NASA's Goddard Space Flight Center (GSFC) in Greenbelt, Maryland vol 2, Issue November. https://www.usgs.gov/landresources/nli/landsat/landsat-7-data-users-handbook

Landsat 8 Data Users Handbook (2019) Landsat Project Science Ofce at NASA's Goddard Space Flight Center (GSFC) in Greenbelt, Maryland, vol 8, Issue November. https://www.usgs.gov/landresources/nli/landsat/landsat-8-data-users-handbook

Mas JF, Flores JJ (2008) The application of artificial neural networks to the analysis of remotely sensed data. Int J Remote Sens 29(3):617–663. https://doi.org/10.1080/01431160701352154

Mberu B, Béguy D, Ezeh AC (2017) Internal Migration, Urbanization and Slums in Sub-Saharan Africa. Africa's Population: In Search of a Demographic Dividend. Springer International Publishing, Cham, pp 315–332

Mishra VN, Rai PK (2016) A remote sensing aided multi-layer perceptron-Markov chain analysis for land use and land cover change prediction in Patna district (Bihar), India. Arab J Geosci 9(4):249. https://doi.org/10.1007/s12517-015-2138-3

Nurwanda A, Honjo T (2020) The prediction of city expansion and land surface temperature in Bogor City, Indonesia. Sustain Cities Soc 52:101772. https://doi.org/10.1016/j.scs.2019.101772

Panday PK (2020) Urbanization and Urban Poverty in Bangladesh. In: The Face of Urbanization and Urban Poverty in Bangladesh. Springer, pp 43–55

Pawe CK, Saikia A (2018) Unplanned urban growth: land use/land cover change in the Guwahati Metropolitan Area. India Geogr Tidsskr J Geogr 118(1):88–100. https://doi.org/10.1080/00167223.2017.1405357

Peng J, Ma J, Liu Q, Liu Y, Li Y, Yue Y (2018) Spatial-temporal change of land surface temperature across 285 cities in China: an urban-rural contrast perspective. Sci Total Environ 635:487–497. https://doi.org/10.1016/j.scitotenv.2018.04.105

Qin Z, Karnieli A, Berliner P (2001) A mono-window algorithm for retrieving land surface temperature from Landsat TM data and its application to the Israel-Egypt border region. Int J Remote Sens 22(18):3719–3746. https://doi.org/10.1080/01431160010006971

Rahman M, Ningsheng C, Mahmud GI, Islam MM, Pourghasemi HR, Ahmad H, Habumugisha JM, Washakh RMA, Alam M, Liu E, Han Z, Ni H, Shufeng T, Dewan A (2021) Flooding and its relationship with land cover change, population growth, and road density. Geosci Front 12(6):101224. https://doi.org/10.1016/j.gsf.2021.101224

Raja DR, Hredoy MSN, Islam MK, Islam KMA, Adnan MSG (2021) Spatial distribution of heatwave vulnerability in a coastal city of Bangladesh. Environ Challenges 4(March):100122. https://doi.org/10.1016/j.envc.2021.100122

Rikimaru A, Roy PS, Miyatake S (2002) Tropical forest cover density mapping. Trop Ecol 43(1):39–47

Rouse JW, Haas RH, Schell JA, Deering DW (1974) Monitoring vegetation systems in the Great Plains with ERTS. NASA Spec Publ 351(1974):309

Roy S, Pandit S, Eva EA, Bagmar MSH, Papia M, Banik L, Dube T, Rahman F, Razi MA (2020) Examining the nexus between land surface temperature and urban growth in Chattogram Metropolitan Area of Bangladesh using long term Landsat series data. Urban Clim 32(November 2019):100593. https://doi.org/10.1016/j.uclim.2020.100593

Roy B, Bari E, Nipa NJ, Ani SA (2021) Comparison of temporal changes in urban settlements and land surface temperature in Rangpur and Gazipur Sadar, Bangladesh after the establishment of city corporation. Remote Sens Appl Soc Environ 23:100587. https://doi.org/10.1016/j.rsase.2021.100587

Sannigrahi S, Bhatt S, Rahmat S, Uniyal B, Banerjee S, Chakraborti S, Jha S, Lahiri S, Santra K, Bhatt A (2018) Analyzing the role of biophysical compositions in minimizing urban land surface temperature and urban heating. Urban Clim 24:803–819. https://doi.org/10.1016/j.uclim.2017.10.002

Schalkoff RJ (1997) Artificial neural networks. McGraw-Hill Higher Education

Sharma R, Nehren U, Rahman SA, Meyer M, Rimal B, Aria Seta G, Baral H (2018) Modeling land use and land cover changes and their effects on biodiversity in Central Kalimantan, Indonesia. Land 7(2):57. https://doi.org/10.3390/land7020057

Shi Y, Zhang Y (2018) Remote sensing retrieval of urban land surface temperature in hot-humid region. Urban Clim 24:299–310. https://doi.org/10.1016/j.uclim.2017.01.001

Silva E, Clarke K (2002) Calibration of the SLEUTH urban growth model for Lisbon and Porto, Portugal. Comput Environ Urban Syst 26(6):525–552. https://doi.org/10.1016/S0198-9715(01)00014-X

Sobrino JA, Jiménez-Muñoz JC, Paolini L (2004) Land surface temperature retrieval from LANDSAT TM 5. Remote Sens Environ 90(4):434–440. https://doi.org/10.1016/j.rse.2004.02.003

Soydan O (2020) Effects of landscape composition and patterns on land surface temperature: Urban heat island case study for Nigde. Turkey Urban Clim 34:100688. https://doi.org/10.1016/j.uclim.2020.100688

Srivastava PK, Han D, Rico-Ramirez MA, Bray M, Islam T (2012) Selection of classification techniques for land use/land cover change investigation. Adv Sp Res 50(9):1250–1265. https://doi.org/10.1016/j.asr.2012.06.032

Story M, Congalton RG (1986) Accuracy assessment: a user's perspective. Photogramm Eng Remote Sensing 52(3):397–399

Tariq A, Riaz I, Ahmad Z, Yang B, Amin M, Kausar R, Andleeb S, Farooqi MA, Rafiq M (2020) Land surface temperature relation with normalized satellite indices for the estimation of spatio-temporal trends in temperature among various land use land cover classes of an arid Potohar region using Landsat data. Environ Earth Sci 79(1):1–15. https://doi.org/10.1007/s12665-019-8766-2

Trotter L, Dewan A, Robinson T (2017) Effects of rapid urbanisation on the urban thermal environment between 1990 and 2011 in Dhaka Megacity, Bangladesh. AIMS Environ Sci 4(1):145–167. https://doi.org/10.3934/environsci.2017.1.145

Ullah S, Tahir AA, Akbar TA, Hassan QK, Dewan A, Khan AJ, Khan M (2019) Remote sensing-based quantification of the relationships between land use land cover changes and surface temperature over the lower Himalayan Region. Sustain 11(19):5492. https://doi.org/10.3390/su11195492

USGS (2016) Landsat 8 Data Users Handbook. Greenbelt, Maryland

Voogt JA, Oke TR (2003) Thermal remote sensing of urban climates. Remote Sens Environ 86(3):370–384. https://doi.org/10.1016/S0034-4257(03)00079-8

Wang C, Li Y, Myint SW, Zhao Q, Wentz EA (2019) Impacts of spatial clustering of urban land cover on land surface temperature across Köppen climate zones in the contiguous United States. Landsc Urban Plan 192:103668. https://doi.org/10.1016/j.landurbplan.2019.103668

Wurm M, Taubenböck H (2018) Detecting social groups from space–Assessment of remote sensing-based mapped morphological slums using income data. Remote Sens Lett 9(1):41–50. https://doi.org/10.1080/2150704X.2017.1384586

Xu H (2006) Modification of normalised difference water index (NDWI) to enhance open water features in remotely sensed imagery. Int J Remote Sens 27(14):3025–3033. https://doi.org/10.1080/01431160600589179

Xue Z, Hou G, Zhang Z, Lyu X, Jiang M, Zou Y, Shen X, Wang J, Liu X (2019) Quantifying the cooling-effects of urban and peri-urban wetlands using remote sensing data: case study of cities of Northeast China. Landsc Urban Plan 182:92–100. https://doi.org/10.1016/j.landurbplan.2018.10.015

Yohannes H, Soromessa T, Argaw M, Dewan A (2021) Impact of landscape pattern changes on hydrological ecosystem services in the Beressa watershed of the Blue Nile Basin in Ethiopia. Sci Total Environ 793:148559. https://doi.org/10.1016/j.scitotenv.2021.148559

Zha Y, Gao J, Ni S (2003) Use of normalized difference built-up index in automatically mapping urban areas from TM imagery. Int J Remote Sens 24(3):583–594. https://doi.org/10.1080/01431160304987

Zhou X, Wang Y (2011) Dynamics of land surface temperature in response to land-use/cover change. Geogr Res 49(1):23–36. https://doi.org/10.1111/j.1745-5871.2010.00686.x